HYDRODYNAMIC HULL FORM DESIGN SPACE EXPLORATION OF LARGE MEDIUM-SPEED CATAMARANS USING FULL-SCALE CFD

(DOI No: 10.3940/rina.ijme.2015.a3.331)

M Haase, J R Binns, **N Bose**, Australian Maritime College, University of Tasmania, Australia, **G Davidson**, Revolution Design Pty Ltd, Australia, **G Thomas**, University College London, UK, and **S Friezer**, Stuart Friezer Marine, Denmark

SUMMARY

Large medium-speed catamarans are a new class of vessel currently under development as fuel-efficient ferries for sustainable fast sea transportation. Appropriate data to derive design guidelines for such vessels are not available and therefore a wide range of demihull slenderness ratios were studied to investigate the design space for fuel-efficient operation. Computational fluid dynamics for viscous free-surface flow simulations were utilised to investigate resistance properties of different catamaran configurations having a similar deadweight at light displacement, but with lengths ranging from 110 m to 190 m. The simulations were conducted at full-scale Reynolds numbers ($\log(Re) = 8.9 – 9.6$) and Froude numbers ranged from $Fr = 0.25$ to 0.49. Hulls of 130 m and below had high transport efficiency below 26 knots and in light loading conditions while hulls of 150 m and 170 m showed benefits for heavier displacement cases and speeds up to 35 knots. Furthermore, the study concluded that the lowest drag was achieved with demihull slenderness ratios between 11 and 13.

NOMENCLATURE

CFD	computational fluid dynamics
DTMB 5415	David Taylor Model Test Basin combatant model
ITTC	International Towing Tank Conference
HEAVY	indicates heavy displacement case
LIGHT	indicates light displacement case
MEDIUM	indicates medium displacement case
RANSE	Reynolds-Averaged Navier-Stokes Eqn
SST	shear stress transport
dh	indicates values for single demihull
exp	indicates value from model test
oa	indicates values for entire vessel
A_T/A_X	transom immersion ratio (-)
B	beam (m)
C_B	block coefficient (-)
C_P	prismatic coefficient (-)
C_T	total resistance coefficient (-)
dwt	deadweight tonnes (t)
Fr	length Froude number(-)
g	gravitational constant (m s^{-2})
L	length of vessel (m)
$L/\nabla^{1/3}$	slenderness ratio (-)
$P_{installed}$	installed engine power (MW)
Re	Reynolds number (-)
R_T	total resistance (N)
s	separation of demihull centrelines (m)
s/L	demihull separation ratio (-)
S_W	wetted surface area (m^2)
T	draft (m)
TE	transport efficiency $(dwt \times g \times U)/P_{installed}$
V	velocity (m s^{-1})
$y+$	dimensionless first cell height (-)
ε	relative deviation (-)
$\eta_{propulsion}$	overall propulsive efficiency (-)
ρ	density of water (kg m^{-3})
∇	volumetric displacement (m^3)

1. INTRODUCTION

Large medium-speed catamarans are a new class of ships for sustainable RoPax transportation which are a development of current high-speed catamarans. Contemporary high-speed catamarans are characterised by two demihulls with a large superstructure to accommodate the payload. They are propelled by waterjets, have a length of up to 125 m and operate at speeds of 40 knots and above, usually at Froude numbers of $Fr = 0.6 – 1.0$. Compared to monohulls the main advantages comprise high transverse stability and large deck areas in conjunction with slender demihulls that enable low wave-making resistance and low added resistance in waves, so that combined with good manoeuvrability [1] they provide effective fast sea transportation. However, the high speeds of these craft are not desirable from an environmental point of view [2].

The continual increase in fuel costs, society's increasing awareness of environmental sustainability, and official regulations to limit emissions, such as MARPOL 73/78 Annex VI [3], have raised the demand for highly fuel-efficient vessels. It is proposed that using the specific low-drag advantages of high-speed catamarans at lower operating speeds would provide more efficient vessels with low fuel usage. Nevertheless, little is known about most appropriate hull form in this lower speed regime for vessels that have traditionally been designed and operated at high Froude number. So this study investigated appropriate macro design parameters for medium-speed catamarans to provide maximum fuel-efficiency through minimising resistance.

Demihull slenderness ratio ($L/\nabla_{dh}^{1/3}$) and demihull separation (s/L) have been found to be two of the most important design parameters influencing the resistance of fast displacement catamarans [4],[5] with slender demihulls being the key to minimise environmental impact of catamarans [6]. These two parameters have

Table 1: Main parameters of different catamaran designs. Weight is relative to 130 m base line model.

L	B_{oa}	$L/\nabla_{dh}^{1/3}$			s/L	relative deadweight			relative light-ship weight
[m]	[m]	LIGHT	MEDIUM	HEAVY	[-]	LIGHT	MEDIUM	HEAVY	[-]
110		10.5	9.8	9.2	0.233	0.85	1.52	2.38	0.83
130		11.5	10.8	9.9	0.197	1.00	1.80	2.82	1.00
150	32	12.7	11.9	11.2	0.171	1.07	2.00	3.18	1.19
170		13.8	13.0	12.2	0.151	1.06	2.12	3.47	1.41
190		14.9	14.1	13.2	0.135	0.96	2.14	3.66	1.66

intensively studied using both computational and experimental approaches; principal examples include: [5], [7], [8], [9], [10], [11], [12], [13], [14], [15], [16] and [17]. The outcomes can be summarised that increases in demihull slenderness and demihull separation both lead to a reduction in the total resistance of a vessel around hump speed, although only few [2], [9], [10], [14] investigated very slender hulls with slenderness ratios exceeding 10. Mostly demihull separation ratios of $s/L >$ 0.2 were investigated, with some studies [11], [15], [17], [18] indicating there is a low sensitivity of drag force to changing demihull separation around hump speed for demihulls in very close proximity ($s/L < 0.2$).

In an earlier study [19] the authors showed that systematic hull form series data can be utilised to investigate hull form alterations for large medium-speed catamarans in terms of changing slenderness and demihull separation. Large gains in transport efficiency were achieved when compared to current high-speed catamarans. However, for the targeted speeds of approximately 30 knots, resistance data of sufficiently slender catamarans was unavailable to fully investigate the design space for an energy-efficient design. Therefore, this research aimed to provide resistance data for large catamarans with slender demihulls operating around hump speed to fully explore the design space.

In the current study five different catamaran hulls of L = 110, 130, 150, 170, and 190 m were investigated for three different displacements at Froude numbers from $0.25 < Fr < 0.49$ using computational fluid dynamics (CFD) at full-scale Reynolds numbers ranging from $8.9 < \log(Re) < 9.6$. The slenderness ratio was varied from $9 < L/\nabla^{1/3} < 15$ and the demihull separation from $0.135 < s/L < 2.33$. Whilst he authors have previously shown that this tool is capable of correctly predicting the resistance of catamarans at medium speed [20], further validation was conducted. A base model was validated at model-scale using existing model test results and empirical ship-model correlation lines.

This paper investigated the resistance properties of large medium-speed catamarans using slender demihulls at a relatively low separation to meet the zeitgeist of contemporary fast sea transportation. It aimed to provide a further insight into the hydrodynamic properties of these hulls as well as their performance in terms of transport efficiency when utilised as RoPax ferries.

Table 2: Parameters of catamaran demihulls that solely depend on loading conditions.

Displacement	T [m]	B_{dh} [m]	A_T/A_X	C_B	C_P
LIGHT	3.2		0.21	0.50	0.63
MEDIUM	3.6	3.2	0.25	0.53	0.66
HEAVY	4.1		0.28	0.57	0.68

2. METHODOLOGY

A hull form family was developed and drag prediction using RANSE-based CFD carried out to study the influence of the hull form on the total resistance of large medium-speed catamarans operating around hump. As reported earlier [20] this is an accurate method and superior to other methods such as potential flow solutions [21].

2.1 DESIGN RULES

A novel approach was chosen to study the influence of demihull slenderness on the drag force. The hulls under consideration differ in length (L = 110 – 190 m), but have equal dimensions of overall beam (B_{oa} = 32 m), and demihull beam (B_{dh} = 6.4 m), draft (T_{LIGHT} = 3.2 m) and identical hull form parameters such as block coefficient (C_B = 0.50) and prismatic coefficient (C_P = 0.63) in the light loading condition. Constant demihull beam and draft assured that operational requirements such as canal size and port infrastructure would not be violated. Each hull form was considered at three loading conditions, a light displacement corresponding to T_{LIGHT} = 3.2 m, a medium displacement at a draft of T_{MEDIUM} = 3.6 m and a heavy displacement analogous to a draft of T_{HEAVY} = 4.1 m. The displacement of each hull increased linearly with increasing length. It was assumed that the light weight of the aluminium ship consisted of the weight of the demihulls, components such as superstructure and outfitting, and machinery. While the hull weight was

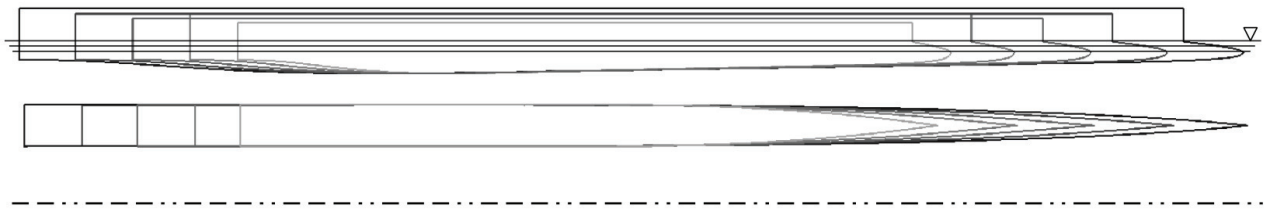

Figure 1: Profile view (top) with corresponding water lines for light, medium and heavy displacement and plan view (bottom) with symmetry line of hulls under consideration.

scaled with length squared, the component weight was scaled linearly with respect to length and weight of the machinery was assumed to be constant for all vessels under consideration. Assuming that the displacement force equals the combination of lightship weight and deadweight, the vessels will have a comparable deadweight at the light displacement. The hull form properties are summarised in Table 1 and 2.

2.1 (a) Implications of Design Rules

For the medium and heavy load case the higher deadweight can be achieved for the longer models, because an increase in length at constant demihull beam increases the waterplane area. For the heavy loading conditions, the shortest hull will be able to carry an additional 180% of its deadweight at light loading conditions, while the longest hull will be able to carry an extra 280% of its deadweight at light loading conditions.

In an earlier study [19], a further requirement was to keep the deck area ($L \times B_{oa}$) constant to compare catamaran designs of different length. It was found to be more practical to keep the overall beam constant. Note though that if the required deck area was insufficient, extra decks could be added for a vessel of this size.

The resulting hull form family featured the 6 models shown in Figure 1 with lengths ranging from 110 to 190 m; varying displacements; different demihull separation ratios (s/L) varying from 0.13 to 0.23; slenderness ratios ($L/\nabla^{1/3}$) ranging from 9 to 15 and transom immersion ratios from 0.21 to 0.28. These three ratios depend on the length of the hulls, whilst the latter two also depend on the loading condition (light, medium, or heavy).

The demihull separation ratio influences the resistance of the catamaran and is one of the most important design parameters for catamarans ([7, 22]. In this study the demihull separation was kept constant but the characteristic demihull separation with respect to vessel length (s/L) decreased as length increased. The demihull separation was altered for the 130 m and 170 m hulls by half a demihull beam in both directions for two Froude numbers (Fr = 0.37, 0.45) at light and heavy displacement, to study its influence on the resistance. For the 130m hull the separation ratio resulted in s/L = 0.15, 0.20, 0.25 and for the 170m hull it was s/L = 0.11, 0.15, 0.19. This enabled the effect of transom immersion and separation ratio on the drag to be investigated as well, since configurations with similar slenderness ratios, but different transom immersions and s/L exist.

The concept of this hull form family allows analysing resistance properties from a hydrodynamic point of view, by considering the drag with respect to the corresponding displacement. Furthermore, it allows looking at it from a design point of view by considering the drag with respect to the deadweight the vessel is able to carry. Latter on is proportional to the inverse of transport efficiency stated in earlier work [19].

2.2 SIMULATION TECHNIQUE

A RANSE-based (Reynolds-Averaged Navier-Stokes Equation) solver featuring transient, viscous, multiphase flow and dynamic mesh motion (*interDyMFoam*) of *OpenFOAM 2.3* was used for simulating the flow around the catamarans. It allows the build-up of free-surface waves and turbulent boundary layers, partial transom immersion and rigid body motions of the vessel to include effects of heave and trim. The SST (shear stress transport) turbulence model was used in accordance with wall functions and an eddy viscosity ratio of 10 was chosen. A symmetry plane was utilised at half demihull separation distance, i.e. the centreline of the complete vessel. All hull forms under consideration were scaled to 2.5 m length during the analysis.

2.2 (a) Mesh Generation

A hybrid mesh consisting of a block-structured background mesh with a hexagonal unstructured mesh featuring hanging nodes in proximity to the vessel was generated using *blockMesh*, *snappyHexMesh* and *refineMesh* from the *OpenFOAM* toolbox. The block-structured background mesh allowed a higher mesh concentration at the free surface and around the vessel with smooth transitions into coarse cells close to the domain boundaries. The mesh was refined around the vessel with special attention paid to refinements between the demihulls, around the transom stern area and within the Kelvin wave angle. The inlet was situated two ship lengths in front of the vessel and the outlet 5 ship lengths aft. Figure 2 shows the principal setup of the mesh in terms of cell level, which is a measure for mesh density. It

ranged from 0 at the bottom of the domain to 4 in close proximity of the hull. Cell size is approximately 2% of vessel length at cell level 0 and the density increased eight-fold with each cell level. The mesh was generated at a 1:4 longitudinal geometric compression and finally stretched to the original aspect ratio to allow the originally cubical cells to be stretched in the flow direction to reduce the cell count. Cubical cells enabled the best performance of *snappyHexMesh* for mesh refinement and surface layer around the hull. Four prismatic layers with 1 mm cell height for the first layer and a 20% cell expansion was used to capture the boundary layer flow, allowing values of $y+ \approx 50$ at model-scale and $y+ \approx 10{,}000$ at full-scale. The total cell count was chosen to assure computational efficiency, accurate results, adequate surface layers and trouble-free meshing.

To keep the mesh comparable between the different hulls of constant length, but different draft and beam, the background mesh was altered to assure a similar number of cells relative to the draft and width. This resulted in an increased cell size for the slenderer hull as the number of cells in the longitudinal direction increased with the aim to achieve cubical cells. The total mesh count varied between 600k – 800k cells.

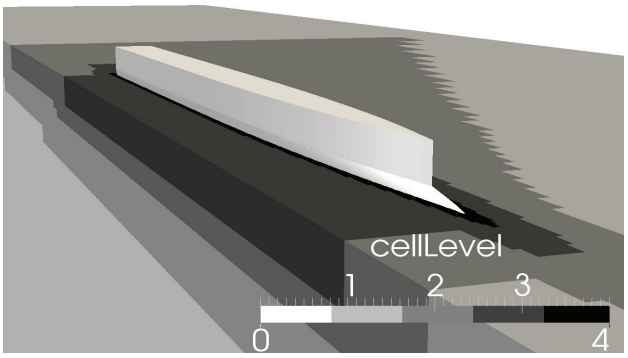

Figure 2: Mesh setup cell density expressed by cell level. Dark shade indicates high mesh density.

2.2 (b) Validation Approach for Full-scale CFD

This numerical study used a hybrid approach based on experimental and empirical data to validate a full scale prediction. Firstly the computational model was validated at model-scale against experimental data to assure that the flow characteristics at model-scale Froude and Reynolds number were successfully replicated.

It was assumed that the accuracy of pressure and wave-making related resistance is independent of Reynolds number and only depends on the size of the cells relative to the length of the hull. The resistance due to shear was compared to established ship-model correlations lines such as ITTC ‘57 and Grigson [23], where an acceptable agreement was assumed to indicate the adequate decomposition of the total drag force into normal and tangential stresses.

Full-scale Reynolds numbers were achieved by altering the viscosity of the fluid while the geometric properties remained at the model-scale. If the resulting shear force was in good agreement with empirical data it was assumed that the resulting total drag force is physically adequate.

2.2 (c) Experimental Validation at Model-scale

The 130 m hull was the base model of this hull form family and it had previously been tested in the Australian Maritime College towing tank with results presented previously [2], [14]. For this study the drag force at Froude numbers of Fr = 0.28, 0.37 and 0.45 was compared to the experimental results at a light and heavy displacement, respectively. These three speeds represent consecutive hump, hollow and hump in the resistance curve with the latter one being the main hump.

3. RESULTS

The following section includes the results of the validation of the novel method for full-scale CFD as well as the outcomes from the design space exploration. A discussion follows in section 4.

3.1 VALIDATION

Good agreement was seen for the drag force determined in simulations at model-scale Reynolds numbers when compared to the measurements in model test experiments for the speeds under consideration. The relative deviation was defined by

$$\varepsilon = \left(\frac{R_{Texp} / \nabla_{\exp} - R_{Tcfd} / \nabla_{cfd}}{R_{Texp} / \nabla_{\exp}} \right)$$

A deviation of $\varepsilon < 5\%$ was observed with the numerical prediction generally below the experimental result. For the heavy displacement at Fr = 0.28 the numerical value exceeded the experimental result by 7%, which may be due to the partially ventilated transom at this condition. The shear force coefficient for all three cases was well within the correlation lines of ITTC and Grigson.

Figure 3 shows the absolute values of relative deviation between numerical and experimental results. These values are compared with the median total uncertainties for an unconventional fast displacement hull of 3 m length (DTMB 5415) to include a measure for experimental uncertainty. This data was determined by model test data from different model test facilities and analysed for ITTC [24] and reached 4 – 6% for the speeds under consideration.

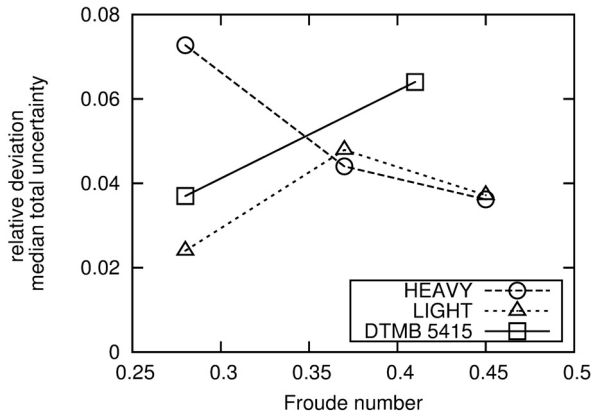

Figure 3: Absolute of relative deviation between CFD and experiments for light and heavy displacement and median total uncertainty of DTMB 5415 model [24].

3.2 HYDRODYNAMIC PROPERTIES OF SLENDER HULLS

3.2 (a) Total Resistance Coefficient

Figure 4 shows the total resistance coefficient (C_T) of the full-scale ship based on numerical simulations and a consistent variation for changing Froude number and displacement can be observed. The resistance coefficient reduces with increasing slenderness and the hollow and humps in the resistance curve become less pronounced. The resistance coefficient of the hulls of L = 150 – 190 m remain almost unchanged for Fr = 0.40 – 0.49. However the hulls under consideration differ in displacement and wetted surface area and no conclusions towards appropriate performance on the most appropriate hull form can be drawn.

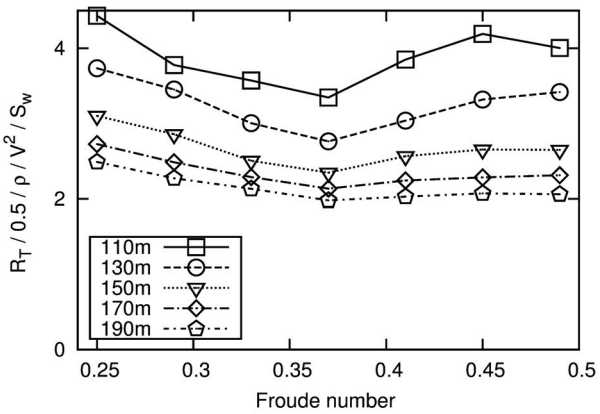

Figure 4: Total resistance coefficient for medium speed hull forms at medium displacement with respect to Froude number.

3.2 (b) Non-dimensional drag

Figure 5 shows the drag non-dimensionalised by volumetric displacement, density, gravity and Froude number squared for the medium displacement case with respect to Froude number:

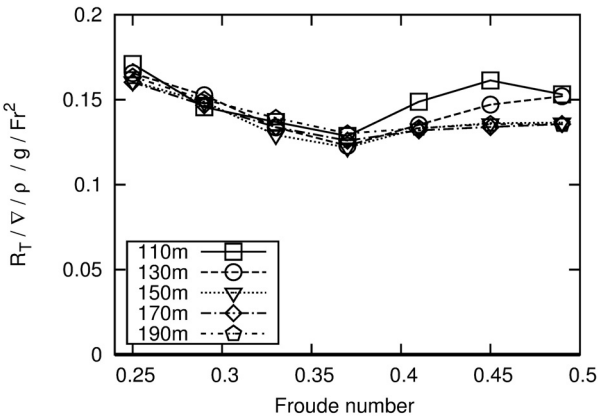

Figure 5: Drag non-dimensionalised by buoyancy force and divided by Froude number squared presented with respect to Froude number

$$R_T' = \frac{R_T}{\nabla \times \rho \times g \times Fr^2}$$

This graph shows that the non-dimensional resistance decreases for increasing Froude number and reaches a minimum at Fr = 0.37 and increases at a varying gradient thereafter, whereas the 110 m and the 130 m hull show higher gradients. This is also the situation for the light and heavy displacements, but for Fr < 0.37 the 190 m hull shows a higher normalised resistance at the light displacement and the 110 m and 130 m hull at the higher displacement case.

The gradient of the resistance curve between Fr = 0.25 – 0.37 increases with increasing displacement. The minimum value at Fr = 0.37 is lowest for the light displacement followed by the medium and heavy displacement, vary from 0.12 – 0.15 across all hulls and displacements.

For the light displacement case the hulls of 110 – 150 m from Fr = 0.25 – 0.37 are grouped together, but are branching for higher speeds whereas the longer hulls have more beneficial resistance behaviour. For the medium displacement a grouping of the curves for L = 130 – 190 m was seen and for the heavy displacement a grouping of L = 150 – 190 m can be observed. Hulls outside that group had a higher normalised resistance.

3.2 (c) Shear Force

Figure 6 shows the shear force coefficient for each displacement compared to the ship-model correlation lines of ITTC and Grigson and the values predicted in this study are well between the boundaries of the two lines. Furthermore a dependency on the Froude number can be observed for all cases under consideration. The shear force coefficient increased for the light displacement mode and decreased for the heavy displacement case compared to the medium case, but still remained between the two empirical lines.

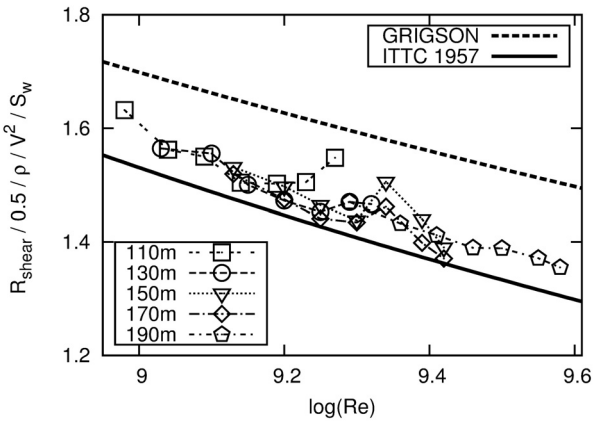

Figure 6: Shear force coefficient for light, medium and heavy displacement compared to ship-model correlation lines of Grigson and ITTC.

3.2 (d) Pressure Drag

The fraction of the pressure drag varied between 0.25 – 0.60 of the total drag at the light displacement. It ranged between 0.25 – 0.30 for the 190 m hull and between 0.45 – 0.60 for the 110 m hull, whereas the highest values occurred at the highest Froude number (*Fr* = 0.49) for the light displacement and at the lowest Froude number (*Fr* = 0.25) for the heavy displacement. For the medium displacement the relative pressure drag varied from 0.30 – 0.70 and for heavy displacement from 0.35 – 0.75. The lowest value was always observed at *Fr* = 0.37.

3.2 (e) Sinkage and Trim

Figure 7 shows the vessel sinkage for increasing Froude number normalised by vessel length. The sinkage increased for increasing Froude number and is more pronounced for the vessels of shorter length. A maximum is reached around Froude number of *Fr* = 0.45 after that the draft starts to decrease again.

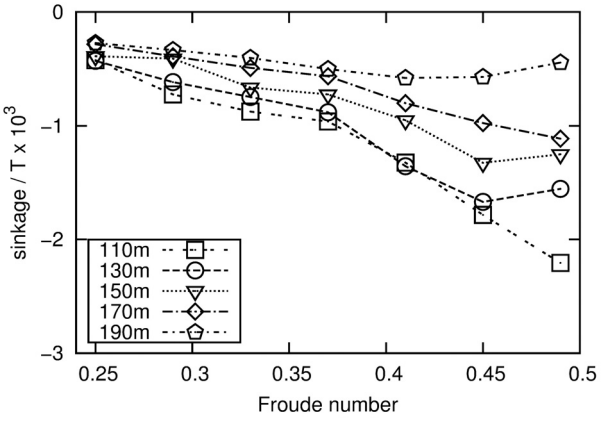

Figure 7: Heave normalised by draft presented with respect to Froude number for medium displacement.

Figure 8 presents the trim angle with respect to Froude number, negative values indicate bow up trim. Trim increases with increasing speed, however absolute values remain small and do not differ significantly between hull shapes. For *Fr* > 0.37 trim increases with a larger gradient for less slender models. Displacement appears to have little effect on the trim angle, but a small increase with increasing displacement was observed.

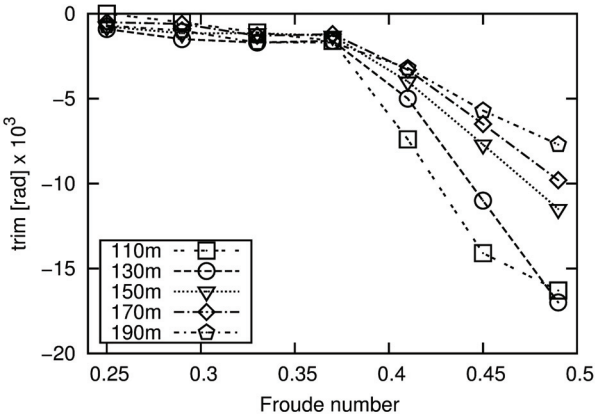

Figure 8: Trim presented with respect to Froude number for medium displacement.

3.2 (f) Free Surface Elevation

Figure 9 shows the free surface elevation around the 130 m model at medium displacement for the full speed range under consideration, where dark grey indicates a wave trough and light grey a wave peak. Black and white corresponds to free surface deformations of 1% of the ship length. At *Fr* = 0.25, characteristic patterns can be seen such as a wave shedding off the bow towards port, humps and hollows between the demihulls and a rooster tail past the transom stern. With Froude numbers increasing to *Fr* < 0.33 this wave pattern becomes more noticeable. For speeds of *Fr* = 0.33 – 0.45 a distinctive wave pattern on the outwards facing side can be observed. One trough leading away from the bow and one around amidships of the demihull are getting more pronounced with increasing speed. A fine crest between these troughs results in a typical pattern for these types of vessels at medium speeds. The two troughs are hardly distinguishable at *Fr* = 0.49 when the boat enters the planing regime.

Between the demihulls and especially at the centre line the formation of back-to-back hollows and peaks can be seen to occur in a more roundish shape rather than distinct crests and troughs. For *Fr* < 0.37 the first hollow is usually more strongly pronounced than the first peak, while at higher Froude numbers the peak appears to be larger than the trough. The first pair of hollow and peak resulting from the superposition of the bow wave move further downstream with increasing Froude number and finally disappear at *Fr* = 0.49 due to the main hollow that forms around the demihulls. The most notable characteristic is the rooster tail seen aft of the transom stern. The depression past the transom increases with increasing Froude number and the angle relative to the demihull centreline of the trailing wave

decreases. An increasing density of the contour lines of the surface elevation indicate a very steep wave and wave breaking is likely to occur, though not in the simulations due to the chosen mesh density. The main features of the wave-pattern agree with those presented by other researchers [15].

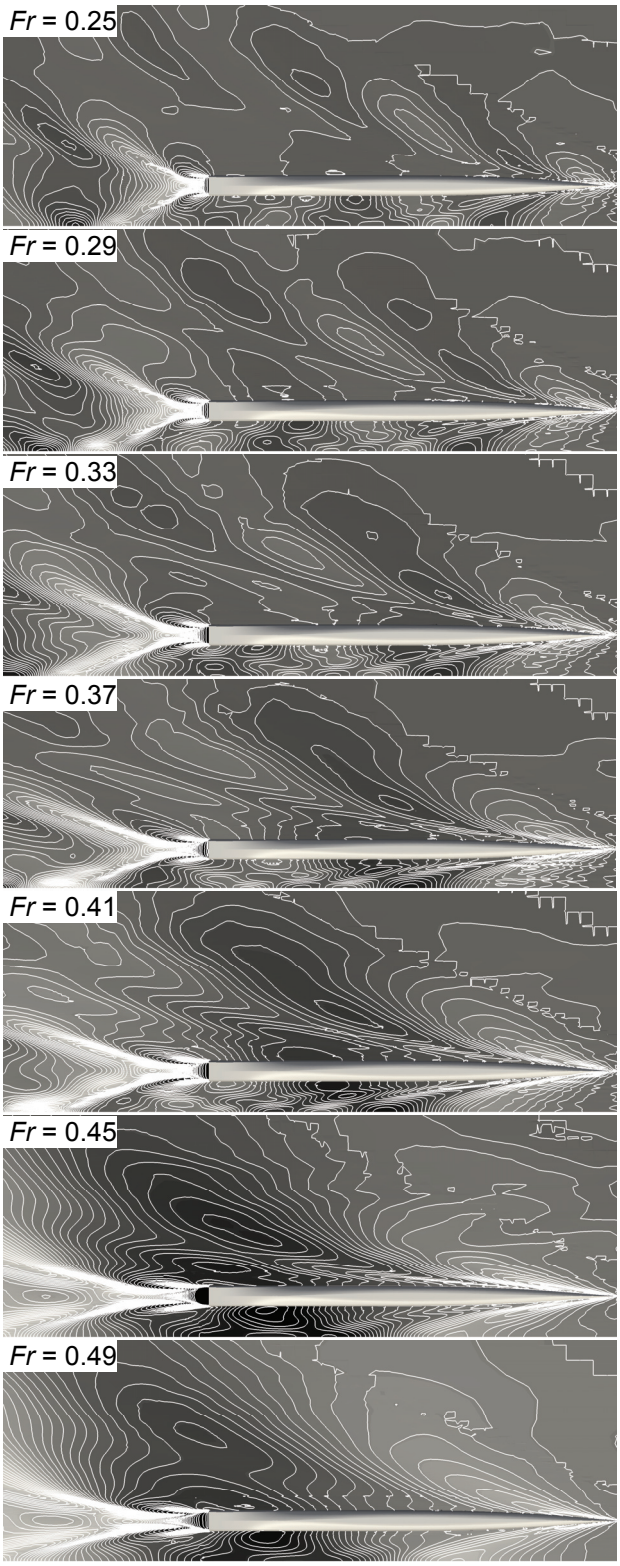

Figure 9: Free surface elevation of 130 m medium-speed catamaran at medium displacement for Fr = 0.25, 0.29, 0.33, 0.37, 0.41, 0.45, and 0.49 from top to bottom.

Figure 10 examines the free surface elevation for medium displacement at Fr = 0.41 for ship length of L = 110 – 190m. The wave height was scaled consistently with respect to ship length and black and white indicate absolute elevations of 1% of the ship length. Whilst the characteristic features of the wave pattern remain unchanged as slenderness increases the wave elevation as well as the rooster tail reduces.

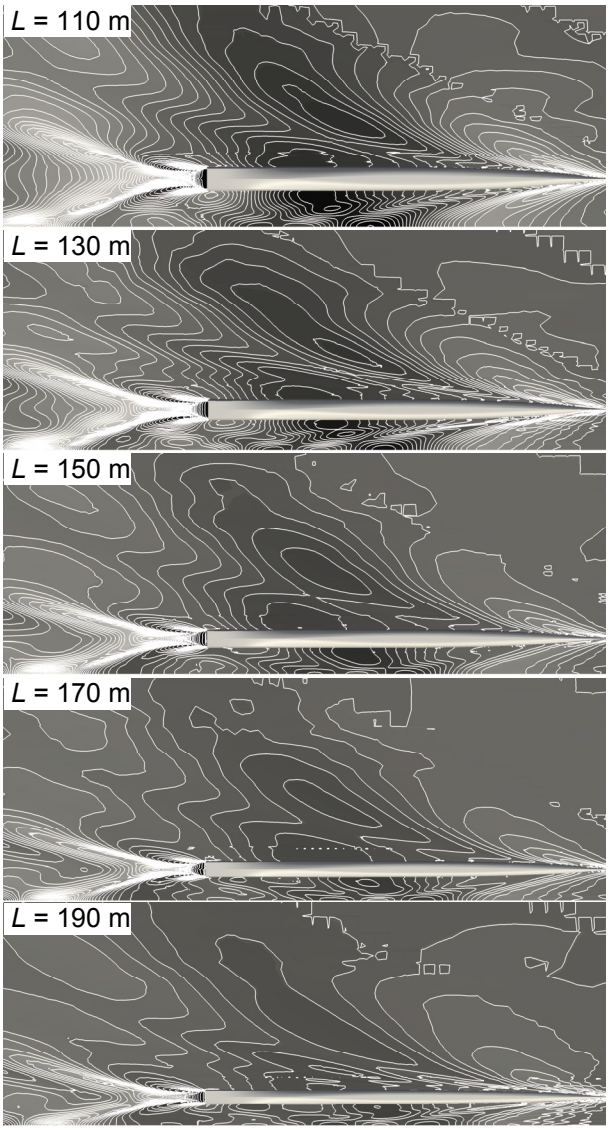

Figure 10: Wave elevation of large medium-speed catamarans at Fr = 0.41 of 110 – 190 m in length at medium displacement (top to bottom).

Finally, the influence of the displacement is shown in Figure 11 for L = 130m at Fr = 0.41. Again the main features of the wave pattern remain constant, but the wave elevation, as well as the rooster tail, increase in magnitude with increasing displacement.

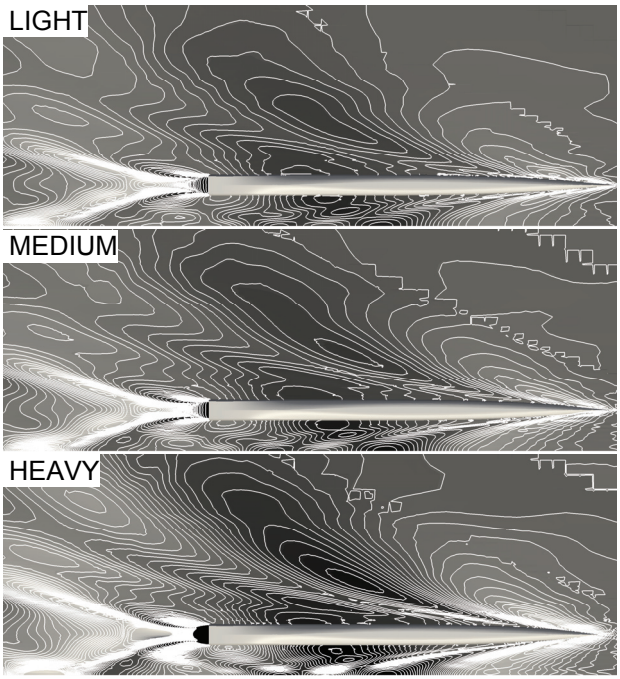

Figure 11: Free surface elevation of 130 m medium-speed catamaran at *Fr* = 0.41 for light (top), medium (middle) and heavy displacement (bottom).

3.2 (g) Demihull Interaction

The demihull separation was varied by a half demihull beam which leads to +/- 10% change in overall beam at constant displacement. An insignificant variation in drag of below 3% for the 130 m and 170m hull at *Fr* = 0 .37, 0.45 for light and heavy displacement was observed and the influence of varying separation on the resistance using the parameters under consideration for such slender hulls was assumed to be small.

3.3 DESIGN SPACE EXPLORATION

In this section the resistance data was interpreted to derive guidelines for the design of large medium speed catamarans with low drag and high transport efficiency. Two approaches are presented: firstly fully non-dimensional representation of the resistance to determine appropriate demihull slenderness ratios at certain Froude numbers and displacements; secondly, the results are presented in terms of transport efficiency to derive the appropriate overall length for a certain operating speed range.

Figure 12 a-c shows the total drag non-dimensionalised by buoyancy force and divided by Froude number square plotted over the slenderness ratio for constant Froude number (*Fr* = 0.29, 0.37, 0.45) at light, medium and heavy displacement. The difference in result for varying displacement is due to the change in transom immersion as the drag force was normalised by the displacement force.

At *Fr* = 0.29 (Figure 12 a), increasing displacement results in a larger dimensionless drag force. The heavy displacement case shows a decreasing resistance with increasing slenderness, but a minimum in the resistance curve cannot be observed. The demihull slenderness ratios under consideration did not include those of minimum resistance.

At *Fr* = 0.37 (Figure 12 b) it was observed that the drag was generally lower than at *Fr* = 0.29, 0.45 and the differences between the three displacement cases was less pronounced than it was at *Fr* = 0.29.

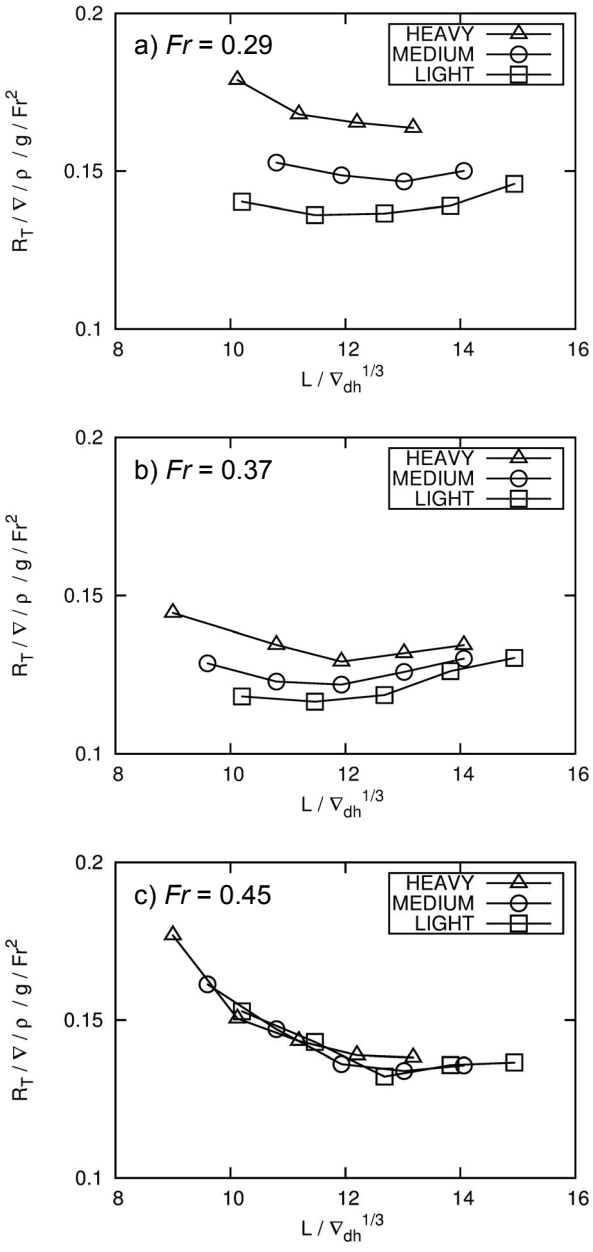

Figure 12: Non-dimensional drag as a function of demihull slenderness ratio for a) *Fr* = 0.29, b) *Fr* = 0.37 and c) *Fr* = 0.45.

Table 3: Minimum achieved non-dimensional drag and corresponding slenderness ratio. Slenderness ranges where normalised drag was within 5% of minimum value

	Fr = 0.29			Fr = 0.37			Fr = 0.45		
	Lowest non-dimensional drag	Corresp. Slendern.	Slendern. w/i 5% of lowest achieved drag	Lowest non-dimensional drag	Corresp. Slendern.	Slendern. w/i 5% of lowest achieved drag	Lowest non-dimensional drag	Corresp. Slendern.	Slendern. w/i 5% of lowest achieved drag
LIGHT	0.137	11.5	10 – 14	0.117	11.5	10.5 – 14	0.132	12.7	12 – 15
MEDIUM	0.147	13.0	11 – 14	0.122	11.9	10.5 – 13	0.134	13.0	11.5 – 14.5
HEAVY	0.164	13.2	11 – 13	0.129	12.2	10 – 13	0.138	13.2	11 – 13.5

3.3 (a) Non-dimensional Analysis

Figure 12 c) indicates that at Fr = 0.45 an increasing slenderness leads to a reduction in drag with a minimum around $L/\nabla^{1/3}$ = 13 observed for all three cases. The difference for the varying displacements is indistinguishable and the drag solely depends on the slenderness ratio with the effect of transom immersion becoming negligible. At this particular Froude number the biggest impact of the slenderness on the resistance can be seen and drag savings of up to 25% can be achieved if a slender hull is used with $L/\nabla^{1/3}$= 13 instead of 9.

The most appropriate slenderness for the three Froude numbers presented varied from 11.5 to 13.2 whereas the difference between the minimum values for the light and heavy displacement varied by 20%, 10% and 5% for Fr = 0.29, 0.37 and 0.45 respectively. The slenderness ratio may be varied up to +/- 2 to be within 5% of the lowest achieved value. See Table 3 for the values of lowest drag, corresponding slenderness ratio and the range of slenderness ratio to remain within 5% of the lowest achieved value. Furthermore, for most cases it was observed that the optimum values of slenderness featuring minimal resistance with respect to buoyancy exist and exceeding the optimum slenderness can lead to an increase in resistance at a similar rate than the decrease at slenderness ratios below the optimum value.

3.3 (b) Transport Efficiency

The performance of a ferry in operation should not only be assessed by its drag with respect to its displacement, but also the drag with respect to its payload or deadweight which can be defined as transport efficiency. In earlier work [19], transport efficiency was defined as:

$$TE = \frac{dwt \times g \times V}{P_{installed}}$$

If we assume that

$$P_{inst} = P_E / \eta_{Propulsion}$$

and

$$P_E = R_T \times V,$$

Transport efficiency can be expressed as

$$TE = \frac{\eta_{Propulsion} \times dwt \times g}{R_T}$$

It was assumed that $\eta_{propulsion}$ = 0.5 and is constant for all speed, hulls and displacements. Therefore, transport efficiency is inversely proportional to the total drag over deadweight.

Figure 13 (a-c) shows the transport efficiency over the speed range from 20 – 35 kn for each displacement. It decreases with increasing speed and reaches higher values at higher displacements. For the light displacement case the transport efficiency of the different length ships ranged from 10.5 at 20 kn to 3.5 at 35 kn. The highest transport efficiency was achieved for the 150 m hull throughout the speed range, with other hulls being capable of reaching within 5% or 10% of the highest value depending on the speed range, only the 190 m hull did not reach within 10% of the highest transport efficiency at any speed. Most appropriate speed ranges for each hull are summarised in Table 4 and Figure 14.

Secondly, for the medium displacement case the transport efficiency varied from 15.5 to 6 over the entire speed range. Again the 150 m hull demonstrated the best performance throughout the speed range and the shortcomings of the 110 m hull and 130 m hulls were noted.

Finally, for the heavy displacement case the transport efficiency ranged from 20 to 8.5 over the speeds under consideration. The 170 m and the 190 m hulls show most beneficial transport efficiencies throughout the all speeds, with major drawbacks for the 110 m and 130 m hull.

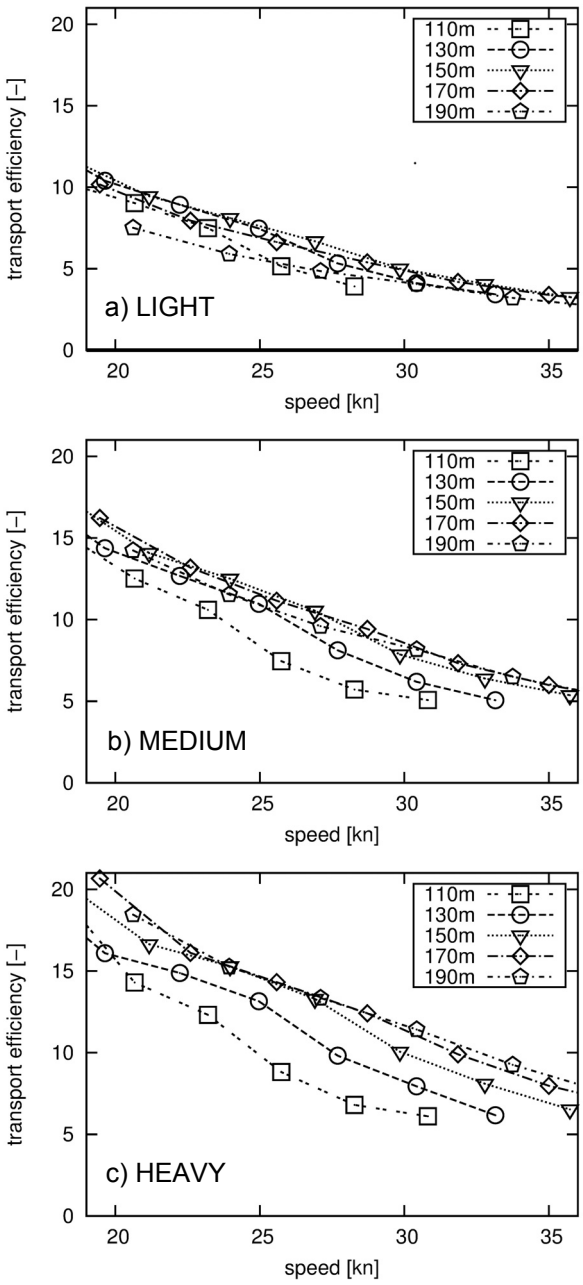

Figure 13: Transport efficiency for light (a), medium (b) and heavy (c) displacement cases with respect to speed.

4. DISCUSSION

4.1 METHODOLOGY

The developed methodology using CFD with full-scale Froude and Reynolds numbers delivered consistent results for all the parameters under investigation to draw conclusions on hull from performance in calm water. Comparing the results of resistance non-dimensionalised by displacement force at model-scale showed good agreement between the simulation and experimental predictions for varying speeds and displacements and a deviation of only 5% may be expected. The resistance of the full-scale ship was not experimentally validated but the values of shear stress were found to be in good correlation with both the ITTC and Grigson ship model correlation lines, which provided sufficient confidence towards the validity of the results of the full-scale simulation.

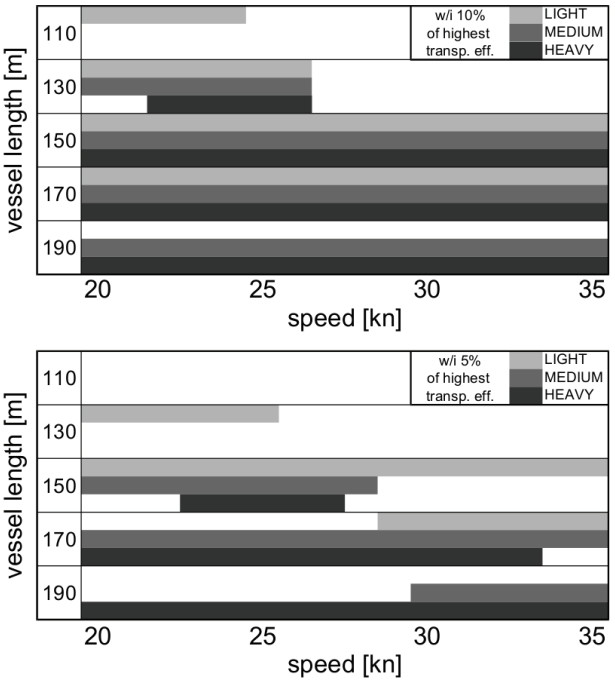

Figure 14: Speed ranges of each vessel configuration is within 10% (top) and within 5% (bottom) of highest achieved transport efficiency.

Table 4: Appropriate speed range for different hull lengths and loading conditions within 10% and 5% of the highest achieved transport efficiency

	Most appropriate speed range [kn]					
	Within 10% of highest transport efficiency			Within 5% of highest transport efficiency		
	LIGHT	MEDIUM	HEAVY	LIGHT	MEDIUM	HEAVY
110 m	20 – 24	N/A	N/A	N/A	N/A	N/A
130 m	20 – 26	20 – 26	22 – 26	20 – 25	N/A	N/A
150 m	20 – 35	20 – 35	20 – 35	20 – 35	20 – 28	23 – 27
170 m	20 – 35	20 – 35	20 – 35	29 – 35	20 – 35	20 – 33
190 m	N/A	20 – 35	20 – 35	N/A	30 – 35	20 – 35

4.2 INFLUENCE ON SHEAR FORCE

Values of shear force coefficients just above the values of the ITTC line agreed with findings fellow investigators [26] who presented shear force coefficients for a high-speed catamaran at Fr = 0.17 – 0.60 and log(Re) = 8.6 – 9.1.

It was found that the shear force was not only influenced by the Reynolds number, but also the Froude number and the displacement. It was seen that the values of Fr = 0.37 are generally closer to the lower of the two ship-model correlation lines, in model-scale as well as in full-scale. The wave elevation along the hull changed for varying Froude numbers and displacements and an influence of the shape of the wetted surface area was assumed. The value for shear force coefficient is generally lower than for a higher displacement and a positive form effect on the shear force was concluded.

4.3 DEMIHULL INTERACTION

The results showed that the change in resistance was not significant for varying demihull separation considering the parameter variation in this study. This agrees with the findings of other researches ([11], [15], [17], [18]) which all presented only minor changes in demihull interference for s/L < 0.2 at Fr < 0.45, but more noticeable changes for larger Froude numbers and larger values of demihull separation value. However, these effects are mainly influenced by the displacement of the hull and the associated wave-making. The slender hulls under consideration will have low wave-making characteristics and therefore penalties in interference drag are expected to be small.

4.4 NON-DIMENSIONAL DRAG FORCE

It was demonstrated that a slenderness ratio around 13 for Fr = 0.29, 0.45 resulted in lowest non-dimensional resistance and of 12 for Fr = 0.37. This is somewhat contrary to the recommendation presented in earlier work [19] where recommendations for slenderness were $L/\nabla^{1/3}$ = 6 – 7 around Fr = 0.30, $L/\nabla^{1/3}$ = 7 – 9 around Fr = 0.37, and $L/\nabla^{1/3}$ = 8 – 9 around Fr = 0.45. As previously discussed those values were guidelines based on built monohull ships and optimum values may change due to advances in technology. Therefore, the present work concludes that these guidelines are not applicable for large medium-speed catamarans because the resistance can be reduced by up to 25% at Fr = 0.45 when using demihulls of higher slenderness.

4.5 TRANSPORT EFFICIENCY

The transport efficiency provides an indication of the efficiency to transport payload from a hydrodynamic point of view. Appropriate designs were identified for highest transport efficiency, depending on the speed and loading condition. In addition, the operational profile needs to be taken into consideration as the target speed and load case may vary during the life cycle of the ship. The charts provided in Figure 13 also give information about the suitability in off-design conditions.

From a production cost perspective a short hull may be preferred to minimise material costs, whereas a longer hull may be preferred to minimise the wave-making for reduced environmental impact such as wave wake at the same transport efficiency.

4.6 FUTURE WORK

A cost comparison model for the full life cycle of the cargo vessel needs to be developed to compare the economic and ecological benefits of differently sized large medium-speed catamarans. Building costs, fuel prices, emissions, port duties and operational profiles have to be taken into account to estimate amortisation times of these vessels.

Using CFD at full-scale Reynolds numbers showed consistent results for a wide range of speeds, slenderness ratios, and drafts, however in future work the validation of this approach will be focussed and possible differences between model and full-scale results will be studied. Furthermore the flow around the transom requires a high resolution for partially wetted transoms, compared to other areas around the hull for accurate resistance prediction. A study of flow characteristics around deep square transom will be undertaken.

5. CONCLUSIONS

This paper reported on a numerical investigation into resistance properties and transport efficiency of large medium-speed catamarans. The vessel length ranged from L = 110 – 190 m, but draft, demihull beam and overall beam were kept constant. Froude numbers varied from Fr = 0.25 – 0.49 which corresponds to speeds of 16 – 41 knots. Furthermore, three different drafts were considered. The study concluded with proposals for design parameters for highest transport efficiency and lowest drag.

Generally transport efficiency was highest for the heavy displacement case and at low speeds. For a certain loading case and speed a vessel length with highest transport efficiency was found. Furthermore, configurations with comparable transport efficiency that was within 5% or 10% of highest achieved value were identified.

The 150 m hull showed best performance at light displacement over the entire speed range, whereas the 170 m performed most advantageously at the heavy displacement case and the 190 m hull at the heavy one. At at certain speed ranges other length hulls were capable of providing comparable transport efficiency. However

for hulls of L = 110, 130 m the transport efficiency was at least 10% below the highest achieved value at speeds beyond 27 knots.

It is concluded that the total resistance coefficient, the difference between humps and hollows in the resistance curve, the absolute values of sinkage and trim, the fraction of pressure drag and the magnitude of the resulting free surface elevation decreased with an increasing demihull slenderness ratio. A hollow in the resistance curve at Fr = 0.37 was identified for all cases where resistance coefficient and pressure drag were at a minimum.

At hump speed (Fr = 0.45) the demihull slenderness appropriate for lowest drag with respect to displacement was around 13 for any transom immersion where a demihull slenderness providing low drag was found at $L/\nabla^{1/3}$ = 11.5 – 13.2 for a wide range of speeds and displacements. $L/\nabla^{1/3}$ may be varied by up to 2 to not exceed the minimal achievable resistance with respect to displacement by 5%.

A change in draft altered hull parameters such as the effective slenderness ratio as well as the transom immersion. However, the effect of the first is small, but latter one negatively influences the drag force at low Froude numbers. This effect deteriorates with increasing speeds and at Fr = 0.45 no significant difference in drag normalised by displacement was seen between different transom immersions. Furthermore, an increase in draft leads to a decrease in shear force coefficient that was related to a changing waterline along the hull at speed.

A variation in demihull separation by a half demihull beam led to changes that are within the uncertainty of the results and no significant influence of minor variations in demihull separation ratio was found which agreed with findings of other researchers.

Future work has been proposed to develop a cost model that takes shipping and investment costs for a full life cycle of a ship into account. Additionally the CFD approach will be further investigated for its validity and the flow around transom sterns studied to improve the prediction of the flow around a partially wetted transoms.

6. ACKNOWLEDGEMENTS

This research has been conducted as part of a collaboration research project between INCAT, Revolution Design, MARIN, Wärtsilä and the Australian Maritime College at the University of Tasmania. It was supported under Australian Research Council's Linkage Projects funding scheme (project number LP110100080). Furthermore the authors would like to thank the Tasmanian Partnership for Advanced Computing (TPAC), especially Matthew Armsby and Kym Hill, for their support with computational resources.

7. REFERENCES

1. YUN, L. and BLIAULT, A., High Performance Marine Vehicles, *Springer Verlag*, 2010
2. DAVIDSON, G, ROBERTS, T. R., FRIEZER, S., DAVIS, M. R., BOSE, N., THOMAS, G., BINNS, J.R., and VERBEEK, R., Maximising Efficiency and Minimising Cost in High Speed Craft, *Proceedings of International Conference on Fast Sea Transportation,* 2011.
3. IMO: MARPOL Annex VI – Prevention of Air Pollution from Ships, 2012.
4. MATSUI, S., SHAO, S.M., WANG, Y. C. and TANAKA, K., The Experimental Investigations on Resistance and Seakeeping Qualities of High-speed Catamarans, *Proceedings of International Conference on Fast Sea Transportation*, 1993.
5. MOLLAND, A.F., WELLICOME, J.F. and COUSER, P.R., Resistance Experiments on as Series of High Speed Displacement Catamarans Forms: Variation of Length-Displacement Ratio and Breadth-Draught Ratio, *Technical report, University of Southampton*, 1994.
6. MCKESSON, C., REMLEY, B., and KARNI, Z.: 'Ferry Environmental Impact', *Canadian Institute of Marine Engineers High Performance Vehicles Conference*, 2000.
7. EGGERS, K., Über die Widerstandsverhältnisse von Zweikörperschiffen, *STG Jahrbuch,* 1955.
8. TASAKI, R., A Note on Wavemaking Resistance of Catamarans, *University of Michigan, Ann Abour*, 1962.
9. SATO, R., NOGAMI, H., SHIROSE, Y., ITO, A., MIYATA, H., MASAOKA, K., KAMAL, E. and TSUCHIYA, Y., Hydrodynamic Design of Fast Ferries by the Concept of Super-Slender Twin Hull, *Proceedings of International Conference on Fast Sea Transportation*, 1991.
10. MIYATA, H., OHOMORI, T. and KAMAL, E.M., Hydrodynamical Design of Super-Slender-Twin-Hull Ferries by CFD Techniques, *Proceedings of International Conference on Fast Sea Transportation*, 1991.
11. TUCK, E.O. and LAZAUSKAS, L., Small, Low Drag, Solar-Powered Monohulls and Multihulls, *Applied Mathematics Technical Report, The University of Adelaide*, 1996.
12. DUBROVSKY, V.A. and LYAKHOVITSKY, A.G., Multi Hull Ships, *Backbone Publishing Company*, 2001.
13. CAPRIO, F. and PENSA, C., Experimental Investigation on two Displacement Catamarans: Systematic Variation of Displacement, Clearance and Stagger, *International Journal of Small Craft Technology*, 2007.
14. DAVIDSON, G., ROBERTS, T. R., FRIEZER, S., THOMAS, G., BOSE, N., DAVIS, M.R. and VERBEEK, R., 130m Wave Piercer Catamaran: A New Energy Efficient Multihull Operating at

Critical Speeds, *Proceedings of International RINA Conference on High Speed Marine Vehicles*, 2011.

15. ZAGHI, S., BROGLIA, R. and DI MASCIO, A., Analysis of the Interference Effects for High-speed Catamarans by Model Tests and Numerical Simulations, *Ocean Engineering*, 2011.
16. SOUTO-IGLESIAS, A., FERNANDEZ-GUTIERREZ, D. and PEREZ-ROJAS, L., Experimental assessment of interference resistance for a Series 60 catamaran in free and fixed trim-sinkage conditions ', *Ocean Engineering*, 2012.
17. BROGLIA, R., JACOB, B., ZAGHI, S., STERN, F., and OLIVIERI, A., Experimental Investigation of Interference Effects for High-speed Catamarans, *Ocean Engineering*, 2014.
18. YEUNG, R. W., POUPARD, G. and TOILLIEZ, J. O., Interference-Resistance Prediction and Its Applications to Optimal Multi-Hull Configuration Design, *Transactions of the Society of Naval Architects and Marine Engineers*, 2004.
19. HAASE, M., DAVIDSON, G., FRIEZER, S., BINNS, J.R., THOMAS, G. & BOSE, N., On the Macro Hydrodynamic Design of Highly Efficient Medium-speed Catamarans with Minimum Resistance, *International Journal of Maritime Engineering*, 2012.
20. HAASE, M., ILIOPULOS, F., DAVIDSON, G., FRIEZER, S., THOMAS, G., BINNS, J.R., BOSE, N., LAVROFF, J., and DAVIS, M.R.: Application of RANSE-based Simulations for Resistance Prediction of Medium-speed Catamarans at Different Scales, *Proceedings of Australasian Fluid Mechanics Conference*, 2012.
21. HAASE, M., DAVIDSON, G., BINNS, J.R., THOMAS, G., BOSE, N., Practical Design Aprroach and Resistance Prediction of Large Medium-speed Catamarans, *Ship Technology Research - Schiffstechnik*, 2013.
22. SAUNDERS, H. E., Hydrodynamics for Ship Design, *Society of Naval Architects and Marine Engineers*, 1957
23. GRIGSON, C.W.B., An accurate Smooth Friction Algorithm and its use in Performance Prediction, *Transactions of the Royal Institution of Naval Architect*, 1993.
24. GORSKI, J., The Resistance Committee – Final Report and Recommendations to the 26th ITTC, *Proceedings of the International Towing Tank Conference*, 2011.
25. HADLER, J. B., CAIN, K. M. & SINGLETON, E. M., On the Effect of Transom Area on the Resistance of high-Speed Catamaran Hulls, *Proceedings of International Conference on Fast Sea Transportation*. 2009.
26. ILIOPULOS, F., LAVROFF, J., DAVIS, M.R., BINNS, J.R., DAVIDSON, G. and VERBEEK, R., Validation For Full-scale RANSE Simulation Of Resistance Prediction For High Speed Catamarans, *Proceedings of International Conference on Fast Sea Transportation*, 2013.

